Available online at www.sciencedirect.com
SCIENCE DIRECT®
Chemical Physics Letters 386 (2004) 132–136
CHEMICAL PHYSICS LETTERS
www.elsevier.com/locate/cplett

Near-infrared to green photon upconversion in Mn^{2+} and Yb^{3+} doped lattices

Christine Reinhard [a,*], Pascal Gerner [a], Fernando Rodríguez [b], Sara García-Revilla [c], Rafael Valiente [c,*], Hans U. Güdel [a]

[a] *Departement für Chemie und Biochemie, Universität Bern, Freiestrasse 3, CH-3000 Bern 9, Switzerland*
[b] *DCITIMAC, Facultad de Ciencias, Universidad de Cantabria, Avda. de los Castros s/n, Santander 39005, Spain*
[c] *Departamento de Física Aplicada, Facultad de Ciencias, Universidad de Cantabria, Avda. de los Castros s/n, Santander 39005, Spain*

Received 14 November 2003; in final form 24 December 2003
Published online: 6 February 2004

Abstract

Yb^{3+} excitation in the near-infrared around 1 μm leads to green Mn^{2+} $^4T_1 \rightarrow {}^6A_1$ luminescence in $CaZnF_4$:Mn^{2+}; Yb^{3+}, Zn_2SiO_4:Mn^{2+}; Yb^{3+} and $SrZnCl_4$:Mn^{2+}; Yb^{3+} at 15 K. In the former two compounds the green upconversion (UC) luminescence is visible by eye up to room temperature. In Cs_3MnBr_5:Mn^{2+}; Yb^{3+} no UC luminescence is observed. The UC mechanism consists of a sequence of ground-state absorption and excited-state absorption steps. The UC efficiency at 15 K is of the order of 1% for laser excitation with 130 mW ($f = 53$ mm focusing lens).

1. Introduction

The observation at low temperatures of visible (VIS) light emission upon near-infrared (NIR) excitation in a number of Yb^{3+} doped Mn^{2+} halides a few years ago came as a big surprise [1]. While photon upconversion (UC) is a common phenomenon in lanthanide doped materials [2–4], it is extremely rare in transition metal ion systems [5]. What made the observation of UC luminescence in a Mn^{2+}/Yb^{3+} crystal most intriguing was its obviously cooperative mechanism. The original excitation step is a $^2F_{7/2} \rightarrow {}^2F_{5/2}$ transition on Yb^{3+} around 980 nm, and the luminescence corresponds to $^4T_{1g} \rightarrow {}^6A_{1g}$ on Mn^{2+}. But Yb^{3+} has no excited-state in the VIS, and the emitting $^4T_{1g}$ in the yellow or red is the lowest excited-state of Mn^{2+}. Systematic studies on Yb^{3+} doped $RbMnCl_3$ [6], $CsMnCl_3$ [7], Rb_2MnCl_4 [8], $CsMnBr_3$ [9], $MnCl_2$ and $MnBr_2$ [10] led to a reasonably consistent picture about the UC mechanism. In all the above compounds Mn^{2+} is octahedrally (O_h) coordinated. In this Letter, we present the results of UC studies on Yb^{3+} doped crystalline compounds containing Mn^{2+} in tetrahedral (T_d) coordination. Light emission from $Mn^{2+}(T_d)$ in various chemical environments is well established in the literature [11–13]. It usually occurs in the green, persists up to room temperature and is used as an activator in some lamp phosphors [14]. Besides Yb^{3+} doped Cs_3MnBr_5, we chose the following lattices doped with both Mn^{2+} and Yb^{3+}: $CaZnF_4$:Mn^{2+} 3%; Yb^{3+} 1%, Zn_2SiO_4:Mn^{2+} 8%; Yb^{3+} 6% and $SrZnCl_4$:Mn^{2+} 1%; Yb^{3+} 1%. We thus have a chemical variation and can study its effect on the UC properties.

2. Experimental

Single crystals of greenish-yellow Cs_3MnBr_5:Yb^{3+} 1% (tetragonal; I4/mcm) and transparent $SrZnCl_4$:Mn^{2+} 1%; Yb^{3+} 1% (scheelite, tetragonal; $I4_1/a$) were grown using stoichiometric amounts of the appropriate alkali earth and transition metal halides by the Bridgman method as described in [15,16], respectively. To obtain single crystals of $CaZnF_4$:Mn^{2+} 3%; Yb^{3+} 1% (scheelite,

* Corresponding authors. Fax: +41-31-631-43-99 (C. Reinhard), +34-94-220-14-02 (R. Valiente).
E-mail addresses: christine.reinhard@iac.unibe.ch (C. Reinhard), valientr@unican.es (R. Valiente).

0009-2614/$ - see front matter © 2004 Elsevier B.V. All rights reserved.
doi:10.1016/j.cplett.2003.12.127

tetragonal, $I4_1/a$) we closely followed the procedure described in [17].

A powder sample of $Zn_2SiO_4:Mn^{2+}$ 8%; Yb^{3+} 6% (willemite, rombohedral $R\bar{3}$) [18] was produced by sintering a mixture of 1.6 ZnO, 1 SiO_2, 0.08 $MnCO_3$, 0.03 Yb_2O_3 for 12 h at 1270 °C as described in [19].

The doping concentrations of Mn^{2+} and Yb^{3+} in all the samples are nominal concentrations. The nominal doping concentrations were chosen such, that significant amounts of neighboring Mn^{2+} and Yb^{3+} ions may be expected (see Section 3.2).

The spectroscopic measurements and the data correction were carried out as described in [20].

3. Results and discussion

3.1. Absorption and luminescence properties

Fig. 1a and b show 15 K absorption and luminescence spectra of $Cs_3MnBr_5:Yb^{3+}$, respectively. The 15 K luminescence band of $Rb_2MnCl_4:Yb^{3+}$ is shown in Fig. 1c for comparison. The richly structured absorption bands in the VIS and near UV of Fig. 1a are readily assigned to d–d transitions of $Mn^{2+}(T_d)$, see the labels in the Figure. The unstructured $^4T_1 \rightarrow {}^6A_1$ luminescence band centered at about 19 000 cm^{-1} is Stokes shifted as expected, see Fig. 1b, and we can estimate an energy for the lowest-energy $^4T_1 \leftrightarrow {}^6A_1$ origin at 20 010 cm^{-1}. It is crucial that this is lower than twice the excitation energy of the UC experiments, see below. The maximum of the $Rb_2MnCl_4:Yb^{3+}$ emission band in Fig. 1c lies at about 16 000 cm^{-1} and is red-shifted by about 3000 cm^{-1} with respect to Cs_3MnBr_5. The red to green shift on going from $Mn^{2+}(O_h)$ to $Mn^{2+}(T_d)$ is the result of a smaller crystal field in the latter, as shown in the inset of Fig. 1.

Fig. 2 shows 15 K luminescence spectra of the four samples excited into the $^2F_{7/2} \rightarrow {}^2F_{5/2}$ transitions of Yb^{3+} in the NIR. Fig. 2b also contains the 300 K spectrum for $CaZnF_4:Mn^{2+}$; Yb^{3+}. All the samples exhibit a strong NIR emission band with a lot of fine structure corresponding to Yb^{3+} $^2F_{5/2} \rightarrow {}^2F_{7/2}$ transitions. In Fig. 2b–d we see, in addition, much weaker luminescence bands in the VIS. No VIS emission can be induced by Yb^{3+} excitation, however, in $Cs_3MnBr_5:Yb^{3+}$, see Fig. 2a. For $CaZnF_4:Mn^{2+}$; Yb^{3+} (Fig. 2b) and $Zn_2SiO_4:Mn^{2+}$; Yb^{3+} (Fig. 2c) the VIS emission consists of broad bands which persist up to room temperature, although with reduced intensity. The green UC emission in these two samples is easily seen by eye at room temperature. In $SrZnCl_4:Mn^{2+}$; Yb^{3+} (Fig. 2d), in addition to the green, there is a red band centered at

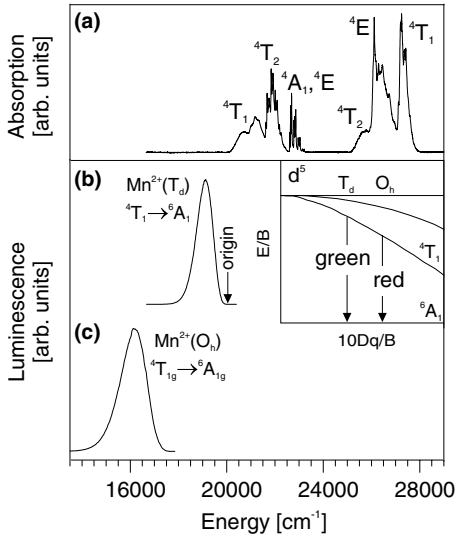

Fig. 1. (a) 15 K absorption spectrum of $Cs_3MnBr_5:Yb^{3+}$, (b) 15 K luminescence spectrum of $Cs_3MnBr_5:Yb^{3+}$ excited at 20 492 cm^{-1} and (c) 13 K luminescence spectrum of $Rb_2MnCl_4:Yb^{3+}$ excited at 19 455 cm^{-1}. The inset shows the Tanabe–Sugano diagram for a d^5 system. The arrows illustrate the red to green shift in the Mn^{2+} luminescence by going from octahedrally (O_h) to tetrahedrally (T_d) coordinated Mn^{2+}.

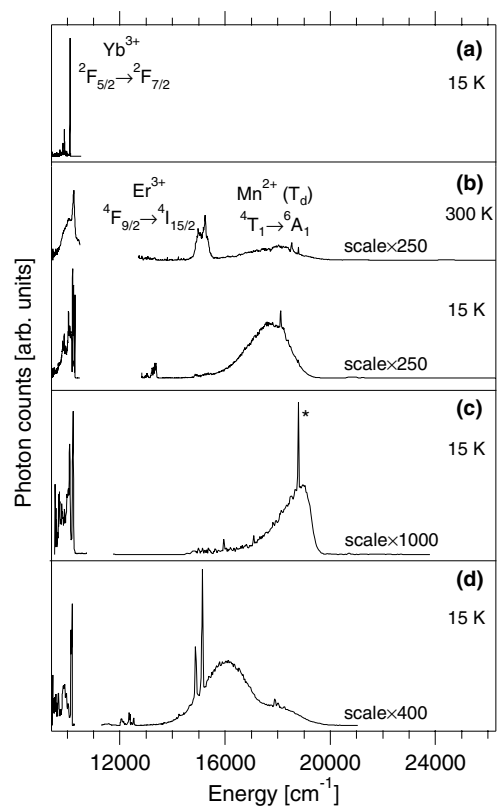

Fig. 2. Survey luminescence spectra at 15 K of (a) $Cs_3MnBr_5:Yb^{3+}$ excited at 10 658 cm^{-1}, (b) $CaZnF_4:Mn^{2+}$; Yb^{3+} excited at 10 557 cm^{-1} (unselective) at RT and 15 K, (c) $Zn_2SiO_4:Mn^{2+}$; Yb^{3+} excited at 10 891 cm^{-1} (unselective), (d) $SrZnCl_4:Mn^{2+}$; Yb^{3+} excited at 10 210 cm^{-1} (selective), respectively. The spectra are excited with a Ti:sapphire laser power of 130 mW (53 mm focusing lens). The scaling factors given in the VIS part of the spectra are calculated for selective excitation into the strongest band of the UC excitation spectrum. The asterisk (∗) denotes a peak due to stray light of the 532 nm pump laser.

about 16 000 cm^{-1}. The sharp $^4F_{9/2} \rightarrow {}^4I_{15/2}$ and $^4S_{3/2} \rightarrow {}^4I_{15/2}$ emissions around 15 000 and 18 000 cm^{-1}, respectively, of an Er^{3+} impurity can be identified in some of the spectra. Fig. 2b shows that the red $^4F_{9/2}$ emission becomes more important at high temperatures, whereas the Mn^{2+} emission decreases. Er^{3+} is known to be a highly efficient UC ion, and ppm impurities imported by the $YbCl_3$ starting material are sufficient to cause these effects. We thus have a clear manifestation of NIR to VIS photon UC in these Yb^{3+} and $Mn^{2+}(T_d)$ codoped crystalline materials. In the lattices $CaZnF_4$, Zn_2SiO_4 and $SrZnCl_4$ we can expect Mn^{2+} to substitute for Zn^{2+} on a site with approximate T_d symmetry. Zn^{2+} and Mn^{2+} have very similar ionic radii for this coordination: 0.60 and 0.66 Å, respectively [21]. In $SrZnCl_4$, Mn^{2+} (0.96 Å) may also substitute for Sr^{2+} (1.26 Å), and we ascribe the UC emission band centered at 16 000 cm^{-1} in Fig. 2d to such a site.

Fig. 3 shows luminescence excitation spectra of $CaZnF_4$:Mn^{2+}; Yb^{3+} at 15 K. In Fig. 3a the Yb^{3+} $^2F_{5/2} \rightarrow {}^2F_{7/2}$ luminescence in the NIR at 9833 cm^{-1} was monitored, while Fig. 3b is the excitation spectrum of the upconverted luminescence measured at 18 904 cm^{-1}. We can confidently assign all these bands to Yb^{3+} $^2F_{7/2} \rightarrow {}^2F_{5/2}$ excitations. Except for the same general energy range the two spectra in Fig. 3a and b have little resemblance, with 3a exhibiting much more fine structure. The $^2F_{5/2}$ state of Yb^{3+} is split into three Kramers doublets by the crystal field. We thus expect three electronic origins. It is known that Yb^{3+} $^2F_{7/2} \rightleftarrows {}^2F_{5/2}$ transitions in solids, both in absorption and emission, exhibit intense vibronic sidebands. Thus the intensity above 10 500 cm^{-1} in Fig. 3a may essentially be vibronic. The structure below 10 300 cm^{-1} clearly indicates the presence of multiple sites. The prominent sharp line at 10 286 cm^{-1} in Fig. 3a must be an electronic origin of a well defined major Yb^{3+} site, whereas, the inhomogeneously broadened bands around 10 200 and 10 230 cm^{-1} are assigned to perturbed sites of Yb^{3+}. The 10 230 cm^{-1} band coincidences with the dominant band of Fig. 3b, and we conclude that this site is by far the most efficient in inducing UC. Careful examination of the excitation spectra of Zn_2SiO_4:Mn^{2+}; Yb^{3+}, $SrZnCl_4$:Mn^{2+}; Yb^{3+}, which are not shown here, reveals very similar behaviour to $CaZnF_4$:Mn^{2+}; Yb^{3+}, with multiple Yb^{3+} sites and UC efficiency only for a minority.

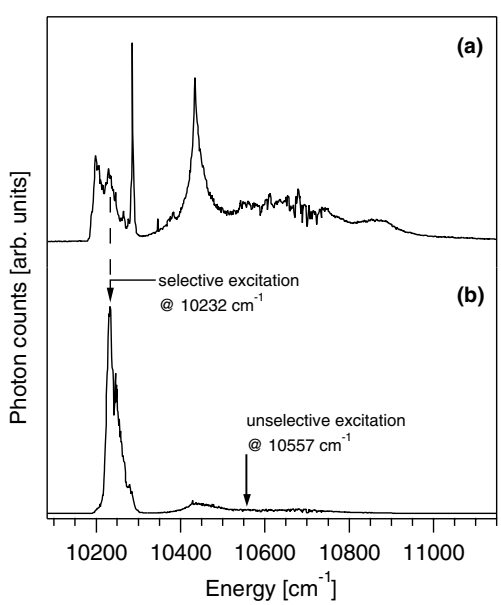

Fig. 3. 15 K excitation spectra monitoring (a) the Yb^{3+} $^2F_{5/2} \rightarrow {}^2F_{7/2}$ luminescence at 9833 cm^{-1} and (b) the upconverted Mn^{2+} $^4T_1 \rightarrow {}^6A_1$ luminescence at 18 904 cm^{-1} in $CaZnF_4$:Mn^{2+}; Yb^{3+}, with the positions for selective and unselective excitations indicated. Both spectra are linearly corrected for the wavelength dependence of the Ti:sapphire laser output.

In all the lattices studied here Yb^{3+} doping requires charge compensation, because there are no trivalent host ions. Yb^{3+} is too large to substitute for tetrahedral Zn^{2+}. Substitution for Ca^{2+} (1.12 Å) and Sr^{2+} (1.26 Å) in $CaZnF_4$ and $SrZnCl_4$, accompanied by Ca^{2+} and Sr^{2+} vacancies for charge compensation, respectively, is conceivable. The Ca^{2+} and Sr^{2+} coordination in these lattices is trigon-dodecahedral, very agreeable for Yb^{3+}. In Zn_2SiO_4 there are interstitial sites which can accommodate Yb^{3+}, with concomitant Zn^{2+} vacancies for charge compensation. In Cs_3MnBr_5, Yb^{3+} doping is much more difficult mainly due to the charge difference between the Cs^+ and the Yb^{3+} ion and the discrepancy between their ionic radii ($Cs^+ = 1.74$ Å and $Yb^{3+} = 0.985$ Å). Therefore, we suppose that only a minute doping level is achieved. This explains the absence of any UC emission in Fig. 2a.

3.2. Upconversion mechanism and efficiency

We can rely on our previous UC work on Yb^{3+} doped octahedral Mn^{2+} compounds [6–9]. With the primary excitation into Yb^{3+} and the resulting Mn^{2+}

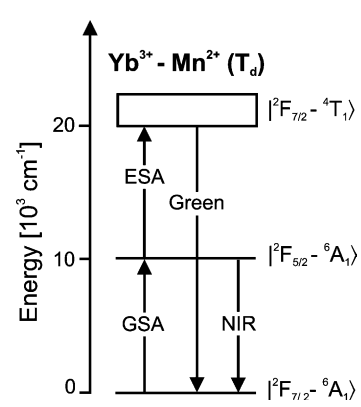

Fig. 4. Schematic representation of the UC process in a simplified Yb^{3+}–Mn^{2+} dimer picture. Straight arrows represent radiative processes.

emission the process is evidently cooperative. For energetic reasons the origin of the UC emission must be less than two times the excitation energy. With an estimated energy about 20 000 cm^{-1} [17] for the lowest origin (20 010 cm^{-1} in Cs_3MnBr_5, see Fig. 1) and excitation not lower than 10 210 cm^{-1} this is fulfilled in all the lattices.

As for the octahedral systems we use the simple dimer picture in Fig. 4 to describe the process. Whereas the first excitation step corresponds to an Yb^{3+} $^2F_{7/2} \rightarrow {}^2F_{5/2}$ ground-state absorption (GSA), the dimer picture is essential to explain the second excitation step. It is an excited-state absorption (ESA) step taking the Yb^{3+}–Mn^{2+} dimer from the $|^2F_{5/2}–^6A_1\rangle$ intermediate to the $|^2F_{7/2}–^4T_1\rangle$ upper excited-state. In the Yb^{3+} doped octahedral Mn^{2+} systems we have clearly shown that the ESA step in the dimer acquires its oscillator strength from exchange interactions [8]. We postulate the same mechanism here. This is based on the close phenomenological analogy to the octahedral systems and also on the measured efficiencies of the process. The integrated VIS(Mn^{2+})/NIR(Yb^{3+}) photon ratios obtained at 15 K are all of the order of 1% for $CaZnF_4$:Mn^{2+}; Yb^{3+}, Zn_2SiO_4:Mn^{2+}; Yb^{3+} and $SrZnCl_4$:Mn^{2+}; Yb^{3+} with 130 mW (53 mm focusing lens) laser power into the strongest band in the UC excitation spectrum (selective excitation). This number is lower than the highest VIS/NIR ratio of 43% at 35 K in Rb_2MnCl_4:Yb^{3+} [8], comparable to VIS/NIR ratios of 2.6% and 0.8% at 12 K for $MnCl_2$:Yb^{3+} and $MnBr_2$:Yb^{3+} [10], respectively, and significantly higher than the VIS/NIR ratio of 0.03% in $CsMnBr_3$:Yb^{3+} at 12 K [9]. The ESA nature of the second excitation step was experimentally confirmed for Zn_2SiO_4:Mn^{2+}; Yb^{3+} by measuring the time evolution after an excitation pulse of 10 ns. The UC emission was found to decay immediately after the pulse, a clear fingerprint of a cooperative process in which both excitation steps are radiative.

With increasing temperature the VIS/NIR photon ratio remains essentially the same for Zn_2SiO_4:Mn^{2+}; Yb^{3+}, whereas for $CaZnF_4$:Mn^{2+}; Yb^{3+} there is a significant drop. We ascribe this mainly to the presence of the Er^{3+} impurities which act as radiative traps for this excitation. Evidence for this is provided in Fig. 2b, where the decrease of the Mn^{2+} $^4T_1$ emission intensity is accompanied by the growth of the Er^{3+} $^4F_{9/2}$ emission intensity with temperature.

4. Conclusions

Green light emission from tetrahedrally coordinated Mn^{2+} ions has been induced in Yb^{3+}/Mn^{2+} codoped crystals of $CaZnF_4$:Mn^{2+}; Yb^{3+}, Zn_2SiO_4:Mn^{2+}; Yb^{3+} and $SrZnCl_4$:Mn^{2+}; Yb^{3+} by Yb^{3+} $^2F_{7/2} \rightarrow {}^2F_{5/2}$ excitation around 980 nm in the NIR. This UC process is reasonably efficient, and persists up to room temperature in $CaZnF_4$:Mn^{2+}; Yb^{3+} and Zn_2SiO_4:Mn^{2+}; Yb^{3+}. This is in contrast to analogous phenomena in Yb^{3+} doped halide compounds with octahedral Mn^{2+} coordination, in which UC is only observed at low temperatures. This difference can be ascribed to the reduced efficiency of nonradiative multiphonon relaxation processes in the lattices with tetrahedral coordination. Their highest phonon energies are lower than for lattices with octahedral coordination. In addition, the $^4T_1$ emission is shifted to the green in the T_d systems, thus increasing the energy gap to the $|^2F_{5/2}–^6A_1\rangle$ intermediate state around 980 nm. In all the lattices studied here Yb^{3+} incorporation requires charge compensation and thus leads to multiple sites with very different UC efficiencies. We are presently exploring new lattices, such as the spinel $MnYb_2S_4$, which offers an ideal site for both partners without any charge compensation.

Acknowledgements

This work was financially supported by the Swiss National Science Foundation. Financial support from Spanish Ministerio de Ciencia y Tecnología (MCyT) is acknowledged (Project No. BFM2001-0695).

References

[1] R. Valiente, O.S. Wenger, H.U. Güdel, Chem. Phys. Lett. 320 (2000) 639.
[2] E. Downing, L. Hesselink, J. Raltson, R.A. McFarlane, Science 273 (1996) 1185.
[3] M.P. Hehlen, K. Krämer, H.U. Güdel, R.A. McFarlane, R.N. Schwartz, Phys. Rev. B 49 (1994) 12475.
[4] M.F. Joubert, S. Guy, S. Cuerq, P.A. Tanner, J. Lumin. 75 (2001) 287.
[5] O.S. Wenger, H.U. Güdel, J. Phys. Chem. B 106 (39) (2002) 10011.
[6] R. Valiente, O.S. Wenger, H.U. Güdel, Phys. Rev. B 63 (2001) 165102/1–165102/11.
[7] R. Valiente, O.S. Wenger, H.U. Güdel, J. Chem. Phys. 116 (2002) 5196.
[8] C. Reinhard, R. Valiente, H.U. Güdel, J. Phys. Chem. B 106 (2002) 10051–10057.
[9] P. Gerner, O.S. Wenger, R. Valiente, H.U. Güdel, Inorg. Chem. 40 (2001) 4534–4542.
[10] P. Gerner, M. Atanasov, P. Bättig, C. Daul, C. Reinhard, H.U. Güdel, private communication.
[11] D.T. Palumbo Jr., J.J. Brown, J. Electrochem. Soc. 117 (9) (1970) 1185.
[12] A.M. Pires, M.R. Davolos, Chem. Mater. 13 (2001) 21.
[13] A.M. Srivastava, H.A. Comanzo, D.A. Doughty, W.W. Beers, Eur. Pat. Appl. (2001) 21.
[14] S. Shinoya, W.M. Yen, Phosphor Handbook, CRC Press, Boca Raton, 1999.
[15] M. Amit, A. Horowitz, E. Ron, J. Makovsky, Isr. J. Chem. 11 (6) (1973) 749.
[16] C. Wickleder, S. Masselmann, G. Meyer, Z. Anorg. Allg. Chem. 625 (1999) 507.

[17] M. Heming, G. Lehmann, K. Recker, F. Wallrafen, Phys. Stat. Sol. B 117 (1983) 271.
[18] P. Hartmann, Z. Kristallogr. 187 (1989) 139.
[19] P. Gerner, C. Fuhrer, C. Reinhard, H.U. Güdel, J. Alloy. Comp., in press.
[20] P. Gerner, K. Krämer, H.U. Güdel, J. Lumin. 102–103 (2003) 112.
[21] R.D. Shannon, Acta Cryst. A32 (1976) 751.